Available online at www.sciencedirect.com
ScienceDirect
Journal of Power Sources 159 (2006) 1169–1185
JOURNAL OF POWER SOURCES
www.elsevier.com/locate/jpowsour

Single-level optimization of a hybrid SOFC–GT power plant

F. Calise [a,*], M. Dentice d' Accadia [a], L. Vanoli [b], M.R. von Spakovsky [c,1]

[a] *DETEC-University of Naples Federico II, P.le Tecchio 80-80125 Naples, Italy*
[b] *DSA-University of Naples Federico II, Via Universitá 100-80055 Portici (NA), Italy*
[c] *Center for Energy Systems Research, Department of Mechanical Engineering, Virginia Polytechnic Institute and State University, Blacksburg, VA 24061, USA*

Received 16 September 2005; accepted 17 November 2005
Available online 28 February 2006

Abstract

The detailed synthesis/design optimization of a hybrid solid oxide fuel cell–gas turbine (SOFC–GT) power plant is presented in this paper. In the first part of the paper, the bulk-flow model used to simulate the plant is discussed. The performance of the centrifugal compressors and radial turbine is determined using maps, properly scaled in order to match the values required for mass flow rate and pressure ratio. Compact heat exchangers are simulated using Colburn and friction factor correlations. For the SOFC, the cell voltage versus current density curves (i.e. polarization curves) are generated on the basis of the Nernst potential and overvoltages. Validation of the SOFC polarization curves is accomplished with data available from Siemens Westinghouse. Both the steam–methane pre-reforming and internal reforming processes are modeled assuming the water–gas shift reaction to be equilibrium-controlled and the demethanization reactions to be kinetically controlled. Finally, a thermoeconomic model is developed by introducing capital cost functions for each plant component. The whole plant is first simulated for a fixed configuration. Then, a synthesis/design optimization of the plant is carried out using a traditional single-level approach. The results of the optimization are presented and discussed.

Keywords: Solid oxide fuel cell; Thermoeconomics; Optimization; Exergy; Simulation

1. Introduction

Solid oxide fuel cells (SOFC) are considered one of the most promising technologies for power production in stationary applications [1]. Hybrid power plants based on SOFCs are expected to reach values of net electrical efficiencies higher than 70% [2–5]. According to many researchers, the best way for using a SOFC in a hybrid power plant is to introduce the cell into a traditional Brayton cycle based on gas turbine (GT) technology [6–10]. In fact, the usual temperature of streams exiting a SOFC is perfectly suitable for the turbine inlet temperature (TIT) required by state-of-the-art turbomachinery [4]. A great number of possible layouts for hybrid SOFC–GT plants have been proposed in the literature [1–10], which include combinations of SOFC stacks, heat exchangers, compressors, gas turbines, pre-reformers, mixers, heat recovery steam generators, and combustors in different arrangements. The performance of these plants have been investigated using a number of different techniques [11–17]. In this paper, the optimal synthesis/design of a specific configuration is performed, using the so-called single-level approach, i.e. an approach which optimizes the system as a whole as opposed to optimizing the system in a multi-level approach which decomposes the system optimization process into a set of multiple subsystem optimizations, the result of which is an optimum for the system that closely approximates that found from the single-level approach [18–20]. The purpose of the single-level approach used here is the total life cycle cost-based optimal synthesis/design of a hybrid fuel cell–gas turbine plant. Thus, the objective function for the optimization is the yearly overall plant cost, i.e. the sum of the amortized capital cost, fuel cost, and thermal energy savings. All of these cost terms are functions of the geometric and thermodynamic decision variables of the plant as described in the simulation model. In this paper, the plant always operates at the design point so that off-design operation is not taken into account during the optimization process. It will be in future work. Detailed cost models are introduced for all components in order to establish a relationship between fuel and capital

* Corresponding author. Tel.: +39 081 7682304; fax: +39 081 2390364.
E-mail address: frcalise@unina.it (F. Calise).
[1] Tel.: +1 540 231 6684; fax: +1 540 231 9100.

0378-7753/$ – see front matter © 2006 Elsevier B.V. All rights reserved.
doi:10.1016/j.jpowsour.2005.11.108

Nomenclature

A_{cr}	reactor cross-area (m^2)
AC	air compressor
c_{fuel}	fuel cost (US$ N^{-1} m^{-3})
C	catalytic burner
C	concentration (kmol m^{-3})
C_i	capital cost of the i component (US$)
e^-	electron flow
E_{act}	activation energy (kJ $kmol^{-1}$)
f_d	by-pass factor at state point 10
f_m	mass flow rate map scaling factor
f_p	pressure ratio map scaling factor
F	Faraday constant (96,485 sA mol^{-1})
FC	fuel compressor
g	Gibbs free energy (kJ $kmol^{-1}$)
GT	gas turbine
h	enthalpy (kJ $kmol^{-1}$)
h_m	average diffusion coefficient (m s^{-1})
HEC	counter-flow heat exchanger
HE1	gas–air heat exchanger
HE2	gas–fuel heat exchanger
HE3	gas–water (air) heat exchanger
HE4	gas–water (fuel) heat exchanger
i	current density (mA cm^{-2})
i_0	exchange current density (mA cm^{-2})
i_l	limiting current density (mA cm^{-2})
IRSOFC	internal reforming solid oxide fuel cell stack
K_{ref}	reforming constant of reaction
K_{sh}	shift constant of reaction
L_r	reactor length (m)
LEV	lower heating value
$\dot{m}$	mass flow rate (kg s^{-1})
$\dot{m}_c$	correct mass flow rate (kg s^{-1})
M	IRSOFC mixer
M1	pre-reformer mixer
M2	gas turbine mixer
M_i	molar mass of the i substance (g mol^{-1})
$\dot{n}$	molar flow rate (kmol s^{-1})
ns	number of species
N	rotor speed (rpm)
N_c	correct rotor speed (rpm)
OF	objective function (US$)
p	partial pressure (bar)
PR	pre-reformer
$\dot{r}_{CH_4}$	demethanization rate function (kmol mm^{-2} s)
R	gas constant (8.3144 kJ $kmol^{-1}$ K)
T	temperature (K)
U_f	fuel utilization factor
V	potential (V)
V_{act}	activation overvoltage (V)
V_{conc}	concentration overvoltage (V)
V_{fuel}	fuel volume flow rate (N m^3 h^{-1})
V_{ohm}	ohmic overvoltage (V)
$\dot{x}$	molar flow rate of CH_4 reacted (kmol s^{-1})
y	molar fraction
$\dot{y}$	molar flow rate of CO reacted (kmol s^{-1})
$\dot{z}$	molar flow rate of H_2 reacted (kmol s^{-1})
0	reference value for pressure or temperature

Greek symbols

α	charge transfer coefficient
δ	thickness (cm)
δ_e	efficiency defect
ζ	amortization factor
λ	resistivity exponential constant (K)
ξ	resistivity pre-exponential constant (Ω cm)
ρ_B	catalyst bulk density (kg m^{-3})
ϕ	inter-collision factor

costs and the geometric and thermodynamic decision variables of the system. Simulation of the system is based on a model previously developed by some of the authors [15–17]. The model is briefly summarized in the first part of the paper, also putting into evidence some improvements introduced with respect to the original version. The optimization problem is then discussed. As a further development of this work, a decomposition strategy (multi-level optimization approach) is also being applied to this same system. It is based on the ILGO/DILGO methods developed and implemented by Muñoz and von Spakovsky [21,22], Rancruel [23], and Rancruel and von Spakovsky [24] and is being applied in order to compare results to those obtained with the single-level approach used in this paper. Results for these optimizations will be discussed in future papers.

2. System layout

Nowadays, at least four different types of SOFC are available (tubular, tubular "high power density", planar and micro-tubular) [1,4]. In spite of the fact that such systems have been studied since the 1970s, until now only a few prototypes have been developed and tested [1]. Siemens Westinghouse is probably one of the most important companies involved in the design and commercialization of hybrid SOFC–GT power plants [25]. This company has installed a 220 kWe hybrid tubular SOFC–GT system at the National Fuel Cell Research Center in California [1,25]. Results of a campaign of performance measurements indicate values of the design point net electrical efficiency to be somewhat lower than the target (52% versus 57%). Furthermore, this particular system demonstrates the huge difficulties encountered in integrating a SOFC with a GT [1]. As a result, much additional development is still required to develop this system further. Thus, an improvement of the coupling between traditional and innovative devices is mandatory [1–4]. Within this scope, the most stringent issue is to find a gas turbine suitable for this application [1]. On the basis of their initial experience, Siemens is now designing new hybrid plants that range from 250 kWe to 10 MWe [1,25] since it is clear that the bigger the size of the plant is, the easier it is to find a GT suitable for the application [26]. In this paper, a 1.5 MWe hybrid power plant is inves-

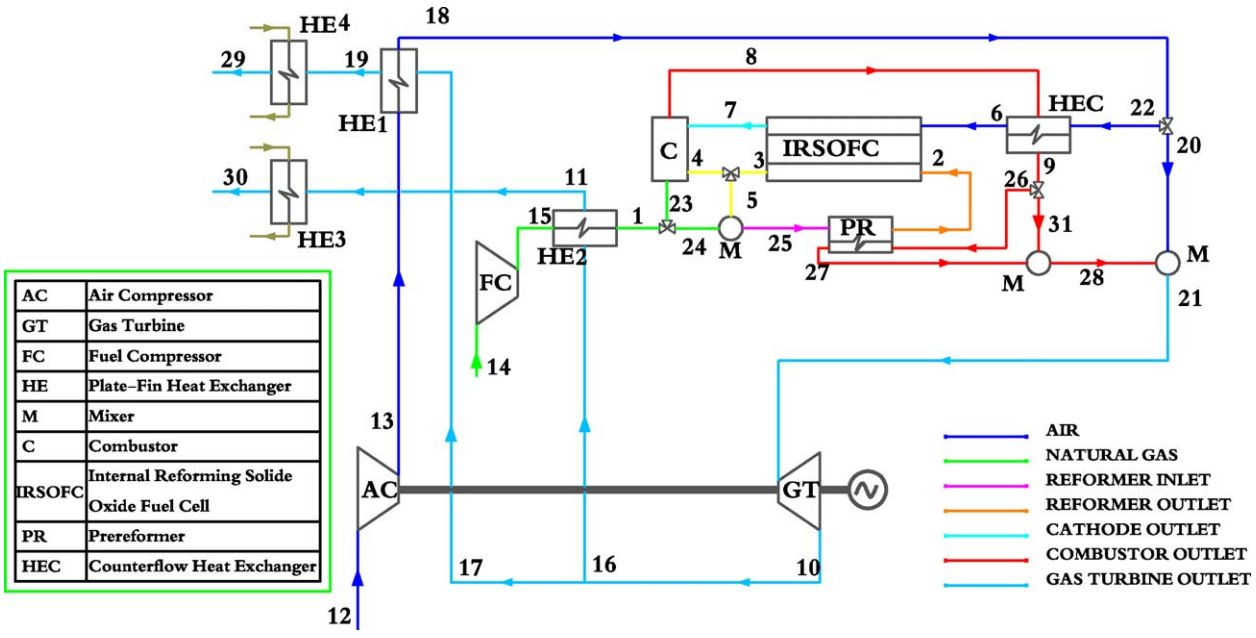

Fig. 1. Plant layout.

tigated, based on an internal reforming tubular SOFC with an anode re-circulation tubular arrangement [1,2,4,10,17,26–29]. This configuration allows one to avoid the use of an expensive external heat recovery steam generator.

In the present paper, the system considered (see Fig. 1) is only analyzed at the design point. Thus, any additional components required for start-up and partial-load operation are not included. Future work will also take into account partial-load operation by introducing time-dependent load curves. The layout proposed for the hybrid plant is shown in Fig. 1. It consists of a centrifugal air compressor (AC); a centrifugal fuel compressor (FC); a plate-fin, air-GT exhaust heat exchanger (HE1); a plate-fin, fuel-GT exhaust heat exchanger (HE2); a radial gas turbine (GT); mixers (M) for anode re-circulation, air by-pass, and pre-reforming by-pass streams; a catalytic burner (C); an internal reforming solid oxide fuel cell (IRSOFC) stack; a pre-reformer (PR); a counter-flow air-SOFC exhaust heat exchanger (HRC); by-pass valves; an electrical generator; an inverter; and two water-exhaust gases, plate-fin heat exchangers (HE3 and HE4). The plant layout includes 31 streams or state points and 14 components. The principle of operation can be summarized as follows:

- Air is compressed by the air compressor (AC) up to the fuel cell operating pressure. The air is then preheated in the plate-fin heat exchanger (HE1) and brought to the cathode inlet of the SOFC stack (state point 18).
- Similarly, the fuel—natural gas—is compressed by the fuel compressor (FC), preheated in the fuel-exhaust gas plate-fin heat exchanger (HE2) and then brought to the anode compartment of the stack (state point 1).
- Both fuel and air can by-pass the fuel cell, i.e. a certain amount of fuel flow can be brought directly to the combustor (C) by-passing the electrochemical reaction occurring within the stack (state point 23), while excess air can be brought to the GT (state point 20).
- At the stack, fuel (state point 24) is mixed with the anode re-circulation stream (state point 5) in order to support the steam reforming reaction in the pre-reformer and in the anode compartment of the fuel cell. The mixture at state point 25 consists of methane and steam. Thus, in the pre-reformer (PR) the first step in the fuel reforming process occurs. The energy required to support the pre-reforming reaction is derived from the hot stream at state point 26. The unreacted fuel at state point 2 is involved in the internal reforming reaction within the anode compartment of the SOFC stack. Here, it is converted into the hydrogen that participates in the electrochemical reaction.
- On the cathode side, air is first preheated by a virtual counter-flow heat exchanger (HEC) and then brought into the annulus (air pipe) of the SOFC where, at the three-phase boundary, the cathode electrochemical reaction occurs [1–4].
- The electrochemical reactions, occurring in the fuel cell, produce dc electrical and thermal energy [1–4]. The first of these is converted into ac current by the inverter; the latter is used by the internal reforming reaction and to heat-up the fuel cell stack.
- The high energy flow rate at state point 8 is first used to preheat air in the counter-flow heat exchanger and then to supply energy to the pre-reforming reaction. This stream at state point 21 enters the gas turbine.
- The expansion in the GT supplies mechanical power and then electric power. The GT outlet stream (state point 10) energy flow rate can be used to preheat both fuel and air flows. Any residual thermal energy left over is available for cogeneration purposes, using two water–gas, plate-fin heat exchangers.

The plant is simulated with the values of its fixed and S/D (synthesis/design, i.e. geometric and thermodynamic) decision

Table 1
Fixed parameters

n	Description	Unit	Value
1	Steam to carbon ratio	–	2
2	Fuel utilization factor	–	0.85
3	Max. SOFC pressure gradient	bar	0.6
4	Max. SOFC temperature gradient	C	60
5	Pre-reformer tube thickness	m	0.0001
6	Max. TIT	C	1250
7	Combustor efficiency	–	0.98
8	Fuel cost	$\$\,N^{-1}\,m^{-3}$	0.2
9	Plate-fin exchange area density	$m^2\,m^{-3}$	1204
10	HE fin conductivity	$W\,m^{-1}\,K^{-1}$	35
11	HE wall-fin conductivity	$W\,m^{-1}\,K^{-1}$	35
12	HE fin thickness	mm	0.152
13	Water inlet temperature	C	60
14	Water outlet temperature	C	80
15	Anode thickness	cm	0.01
16	Cathode thickness	cm	0.22
17	Electrolyte thickness	cm	0.004
18	Interconnect thickness	cm	0.0085

variables described in Tables 1 and 2. Its net electrical power is 1.50 MW, with a 0.561 MW recovered thermal flow. Under these conditions, the initial plant configuration achieves initial energy and exergy electrical efficiencies of 67.9 and 64.9%, respectively. Exergy destruction is mainly due to the HE4 ($\delta_e = 0.255$), SOFC stack ($\delta_e = 0.151$), combustor ($\delta_e = 0.176$) and GT ($\delta_e = 0.142$). These inefficiencies are determined by the chemical and electrochemical conversion processes (IRSOFC and CB), heat exchanges with large temperature differences (HE4) and non-isentropic expansion (GT). State points properties are summarized in Table 3. This table shows the following main results:

- the stack and GT inlet temperatures are close to their design value of 1273 K;
- the second column shows that pressure drops in the plant are often negligible, as a consequence of the gaseous phase of its streams;
- chemical exergy dramatically decreases as a consequence of the reforming and electrochemical reactions, due to its conversion into electricity;
- the SOFC anode outlet methane molar fraction is very low, as a consequence of the high SOFC operating temperature, which also affects the chemical equilibrium of the reforming process;

3. Plant model

The model used to simulate the behavior of the system is a typical lumped-parameter model based on the following assumptions: one-dimensional flow; steady state; no gas leakage; negligible heat losses to the environment; negligible kinetic and gravitational terms. The model is implemented in a computer code developed by the authors and described in detail in [15–17]. However, some improvements were introduced, by removing a part of the simplifying assumptions that were used in the original version. Furthermore, cost models are added for thermoeconomic evaluations. Finally, a genetic algorithm (GA), developed by LENI at the Ecole Polytechnique Fdrale de Lausanne, is used for optimization purposes [30]. The code, including 50 subroutines, was written in MATLAB and is based on a number of built-in functions, tools and externally developed subroutines [31,32]. When possible, equations are solved sequentially, avoiding large non-linear algebraic systems. However, in many cases, the solution of a non-linear system is necessary and is accomplished using the STRSCNE tool [28]. In the version developed for thermoeconomic optimization purposes, the model includes 18 fixed parameters (see Table 1) and 48 S/D decision variables (see Table 2). Fixed parameters, such as the net electric power production, remain constant during the optimization. The S/D decision variables can vary in a given range (usually 30% of the starting value, or "initial" value) and represent the independent variables in the synthesis/design optimization of the system. Obviously, only some of the possible sets of values for the S/D decision variables correspond to actual feasible syntheses/designs. The others are automatically rejected by the code. For any acceptable synthesis/design configuration, the model calculates all energy, entropy, and exergy flow rates entering and leaving each component and the capital cost of each device. The calculation of thermophysical and transport properties are based on temperature-dependent specific heats, viscosities and conductivities and Wilke's Law [15,33,34]. In the following, the most significant aspects of the model are described.

3.1. Electrochemical model

The simulation of the electrochemical phenomena is based on the model described in [15–17] and validated with data provided by Siemens Westinghouse [35]. Even if SOPCs are claimed to be able to electrochemically oxidize not only hydrogen but also carbon monoxide, the likelihood is that the latter is converted through a water–gas shift catalytic reaction and, thus, in this paper it is assumed that the hydrogen reacts electrochemically. The CO is converted into H_2, via the shift reaction, before taking part in the electrochemical reactions given by

$$H_2 + O^{-2} \rightarrow H_2O + 2e^-, \qquad \tfrac{1}{2}O_2 + 2e^- \rightarrow O^{-2} \tag{1}$$

The model is implemented with a number of routines for calculating the open circuit reversible voltage and activation, ohmic and concentration losses. Specifically, the open circuit reversible voltage is calculated on the basis of Nernst equation (Eq. (2)), namely:

$$E = \frac{-\Delta g_0^0}{2F} + \frac{RT}{2F} \log\left(\frac{p_{H_2}\sqrt[2]{p_{O_2}}}{p_{H_2O}}\right) \tag{2}$$

The Gibbs free energy difference of a reaction, at standard pressure (Δg^0) depends dramatically on temperature. This property is calculated taking into account its definition [36] and the

Table 2
Synthesis/design (S/D) decision variables and their values

n	Var.	Unit	Initial	Min	Max	Opt. (1)	Opt. (2)	Opt. (3)	Opt. (4)	Opt. (5)
	c_{fuel}	US\$ $\text{N}^{-1}\,\text{m}^{-3}$	–	–	–	0.10	0.15	0.20	0.25	0.30
1	f_{d}	–	1.00E+00	0.00E+00	1.00E+00	7.88E−01	9.82E−01	1.00E+00	9.94E−01	1.00E+00
2	N_{FC}	rpm	4.00E+04	3.80E+04	4.50E+04	3.97E+04	4.28E+04	3.82E+04	3.94E+04	3.87E+04
3	$f_{\text{m,FC}}$	–	0.00E+00	−2.00E−01	2.00E−01	2.50E−02	1.19E−01	1.48E−01	1.01E−01	1.95E−01
4	$f_{\text{p,FC}}$	–	0.00E+00	−2.00E−01	2.00E−01	−1.17E−02	−1.99E−01	6.85E−02	−1.17E−02	−1.31E−01
6	$L_{\text{c,HE1}}$	m	1.50E+00	1.05E+00	1.95E+00	1.11E+00	1.05E+00	1.05E+00	1.07E+00	1.05E+00
6	$L_{\text{h,HE1}}$	m	1.50E+00	1.05E+00	1.95E+00	1.09E+00	1.05E+00	1.07E+00	1.13E+00	1.05E+00
7	$b_{\text{c,HB1}}$	m	6.35E−03	4.45E−03	8.26E−03	4.85E−03	6.35E−03	4.54E−03	4.89E−03	4.46E−03
8	$b_{\text{h,HE1}}$	m	6.35E−03	4.45E−03	8.26E−03	6.18E−03	6.40E−03	4.45E−03	5.47E−03	7.82E−03
9	$n_{\text{p,HE1}}$	–	2.50E+02	1.75E+02	3.25E+02	1.77E+02	1.75E+02	1.75E+02	1.75E+02	1.82E+02
10	$s_{\text{c,HE1}}$	m	6.35E−03	4.45E−03	8.26E−03	4.65E−03	7.85E−03	8.04E−03	6.64E−03	6.37E−03
11	$s_{\text{h,HE1}}$	m	4.00E−03	2.80E−03	5.20E−03	2.97E−03	2.81E−03	2.83E−03	3.14E−03	2.81E−03
12	$L_{\text{c,HE2}}$	m	5.00E−01	3.50E−01	6.50E−01	5.30E−01	3.98E−01	3.50E−01	4.74E−01	3.64E−01
13	$L_{\text{h,HE2}}$	m	5.00E−01	3.50E−01	6.50E−01	5.20E−01	3.80E−01	4.63E−01	5.51E−01	4.71E−01
14	$b_{\text{c,HB2}}$	m	6.35E−03	4.45E−03	8.26E−03	4.51E−03	8.05E−03	4.85E−03	6.29E−03	6.96E−03
15	$b_{\text{h,HE2}}$	m	6.35E−03	4.45E−03	8.26E−03	5.27E−03	4.70E−03	8.22E−03	7.37E−03	5.66E−03
16	$n_{\text{p,HE2}}$	–	9.00E+00	6.30E+00	1.17E+01	8.00E+00	1.10E+01	8.00E+00	1.10E+01	7.00E+00
17	$s_{\text{c,HE2}}$	m	6.35E−03	4.45E−03	8.26E−03	5.70E−03	4.90E−03	7.73E−03	4.48E−03	7.99E−03
18	$s_{\text{h,HE2}}$	m	4.00E−03	2.80E−03	5.20E−03	3.07E−03	4.14E−03	4.22E−03	3.15E−03	4.51E−03
19	$L_{\text{c,HE3}}$	m	6.00E−01	4.20E−01	7.80E−01	5.39E−01	6.63E−01	7.70E−01	7.79E−01	6.98E−01
20	$L_{\text{h,HE3}}$	m	6.00E−01	4.20E−01	7.80E−01	6.36E−01	7.52E−01	7.76E−01	6.25E−01	7.77E−01
21	$b_{\text{c,HE3}}$	m	6.35E−03	4.45E−03	8.26E−03	4.83E−03	4.69E−03	4.54E−03	5.16E−03	4.46E−03
22	$b_{\text{h,HE3}}$	m	6.35E−03	4.45E−03	8.26E−03	4.46E−03	4.48E−03	4.45E−03	4.53E−03	4.45E−03
23	$N_{\text{AC/GT}}$	rpm	4.00E+04	3.80E+04	4.50E+04	3.96E+04	3.86E+04	3.90E+04	3.99E+04	4.06E+04
24	$n_{\text{p,HE3}}$	–	1.00E+02	7.00E+01	1.30E+02	1.07E+02	1.25E+02	1.30E+02	1.25E+02	1.21E+02
25	$s_{\text{c,HE3}}$	m	6.35E−03	4.45E−03	8.26E−03	4.48E−03	6.43E−03	4.61E−03	7.10E−03	5.59E−03
26	$s_{\text{h,HE3}}$	m	4.00E−03	2.80E−03	5.20E−03	2.97E−03	3.00E−03	2.87E−03	2.86E−03	2.86E−03
27	$L_{\text{c,HE4}}$	m	3.00E−01	2.10E−01	3.90E−01	3.74E−01	3.85E−01	3.71E−01	3.01E−01	3.47E−01
28	$L_{\text{h,HE4}}$	m	3.00E−01	2.10E−01	3.90E−01	3.90E−01	3.37E−01	2.77E−01	3.88E−01	3.89E−01
20	$b_{\text{c,HE4}}$	m	6.35E−03	4.45E−03	8.26E−03	6.50E−03	8.20E−03	6.50E−03	8.00E−03	4.60E−03
30	$b_{\text{h,HE4}}$	m	6.35E−03	4.45E−03	8.26E−03	4.95E−03	6.19E−03	4.52E−03	8.16E−03	7.36E−03
31	$n_{\text{p,HE4}}$	–	1.00E+01	7.00E+00	1.30E+01	1.00E+01	7.00E+00	8.00E+00	1.20E+01	8.00E+00
32	$s_{\text{c,HE4}}$	m	6.35E−03	4.45E−03	8.26E−03	4.47E−03	4.58E−03	4.59E−03	6.46E−03	6.07E−03
33	$s_{\text{h,HE4}}$	m	4.00E−03	2.80E−03	5.20E−03	2.84E−03	2.98E−03	2.80E−03	2.84E−03	5.15E−03
34	D_{inj}	m	7.00E−03	4.90E−03	9.10E−03	4.90E−03	4.91E−03	4.91E−03	4.93E−03	4.90E−03
35	L_{inj}	m	1.00E−01	7.00E−02	1.30E−01	7.12E−02	7.09E−02	7.43E−02	9.76E−02	7.55E−02
36	L_{PR}	m	2.20E−01	1.54E−01	2.86E−01	1.74E−01	2.09E−01	1.67E−01	1.62E−01	1.63E−01
37	f_{PR}	–	3.50E−01	2.50E−01	6.00E−01	2.88E−01	3.14E−01	2.75E−01	2.58E−01	2.78E−01
38	D_{SOFC}	m	1.56E−02	1.09E−02	2.03E−02	1.12E−02	1.11E−02	1.09E−02	1.20E−02	1.10B-02
38	L_{SOFC}	m	1.50E+00	1.05E+00	1.95E+00	1.05E+00	1.06E+00	1.06E+00	1.15E+00	1.05E+00
40	n_{SOFC}	–	1.50E+04	1.05E+04	1.95E+04	1.07E+04	1.06E+04	1.05E+04	1.15E+04	1.05E+04
41	$\dot{m}_{20}/\dot{m}_{18}$	–	0.00E+00	0.00E+00	5.00E−01	0.00E+00	0.00E+00	0.00E+00	0.00E+00	0.00E+00
42	$\dot{m}_{23}/\dot{m}_{1}$	–	0.00E+00	0.00E+00	5.00E−01	1.47E−04	0.00E+00	4.89E−04	1.61E−03	1.64E−03
43	D_{PR}	m	1.56E−02	1.09E−02	2.03E−02	1.80E−02	1.98E−02	1.33E−02	1.48E−02	1.96E−02
44	$f_{\text{m,AC}}$	–	0.00E+00	−2.00E−01	2.00E−01	−1.36E−01	−2.00E−01	−1.87E−01	−1.93E−01	−1.22E−01
45	$f_{\text{p,AC}}$	–	0.00E+00	−2.00E−01	2.00E−01	−7.96E−03	−3.31E−02	8.74E−02	1.10E−02	−1.02E−01
46	$f_{\text{m,CT}}$	–	0.00E+00	−2.00E−01	2.00E−01	−1.77E−01	−9.59E−16	−1.73E−01	−1.11E−01	−2.63E−02
47	$f_{\text{p,GT}}$	–	0.00E+00	−2.00E−01	2.00E−01	9.36E−03	1.61E−02	1.37E−01	1.14E−0L	2.01E−02
48	$\dot{m}_{\text{air}}$	$\text{kg}\,\text{s}^{-1}$	1.76E+00	1.23E+00	2.28E+00	1.76E+00	1.79E+00	1.87E+00	1.84E+00	1.79E+00

Table 3
Thermodynamic properties of the initial configuration

State point	t	p	$\dot{n}_{H_2O}$	$\dot{n}_{CO}$	$\dot{n}_{H_2}$	$\dot{n}_{O_2}$	$\dot{n}_{N_2}$	$\dot{n}_{CO_2}$	$\dot{n}_{CH_4}$	ex_{ch}	ex_{ph}
1	3.64E+02	7.76E+00	0.00E+00	0.00E+00	0.00E+00	0.00E+00	5.62E−05	0.00E+00	2.75E−03	8.20E+05	6.39E+02
2	9.00E+02	7.76E+00	4.75E−03	1.79E−03	3.60E−03	0.00E+00	1.22E−04	2.39E−03	1.79E−03	2.01E+05	1.24E+03
3	9.80E+02	7.76E+00	1.02E−02	1.14E−03	1.71E−03	0.00E+00	1.23E−04	4.82E−03	1.36E−08	4.94E+04	1.11E+03
4	9.80E+02	7.76E+00	4.72E−03	5.27E−04	7.89E−04	0.00E+00	5.62E−05	2.23E−03	6.30E−09	4.94E+04	1.11E+03
5	9.80E+02	7.76E+00	5.50E−03	6.16E−04	9.21E−04	0.00E+00	6.56E−05	2.60E−03	7.35E−09	4.94E+04	1.11E+03
6	6.85E+02	7.48E+00	0.00E+00	0.00E+00	0.00E+00	1.28E−02	4.81E−02	0.00E+00	0.00E+00	1.29E+02	5.10E+02
7	9.80E+02	7.48E+00	0.00E+00	0.00E+00	0.00E+00	7.93E−03	4.81E−02	0.00E+00	0.00E+00	1.70E+02	7.62E+02
8	1.13E+03	7.48E+00	5.51E−03	0.00E+00	0.00E+00	7.27E−03	4.81E−02	2.75E−03	0.00E+00	8.83E+02	9.46E+02
9	1.05E+03	7.48E+00	5.51E−03	0.00E+00	0.00E+00	7.27E−03	4.81E−02	2.75E−03	0.00E+00	8.83E+02	8.63E+02
10	6.46E+02	1.45E+00	5.27E−03	0.00E+00	0.00E+00	7.58E−03	4.82E−02	2.61E−03	0.00E+00	8.28E+02	3.56E+02
11	2.70E+02	1.35E+00	1.34E−04	0.00E+00	0.00E+00	1.92E−04	1.22E−03	6.62E−05	0.00E+00	8.28E+02	9.84E+01
12	2.50E+01	1.00E+00	0.00E+00	0.00E+00	0.00E+00	1.28E−02	4.81E−02	0.00E+00	0.00E+00	1.29E+02	0.00E+00
13	3.05E+02	7.48E+00	0.00E+00	0.00E+00	0.00E+00	1.28E−02	4.81E−02	0.00E+00	0.00E+00	1.29E+02	2.59E+02
14	2.50E+01	1.00E+00	0.00E+00	0.00E+00	0.00E+00	0.00E+00	5.62E−05	0.00E+00	2.75E−03	8.20E+05	0.00E+00
15	2.27E+02	7.76E+00	0.00E+00	0.00E+00	0.00E+00	0.00E+00	5.62E−05	0.00E+00	2.75E−03	8.20E+05	4.38E+02
16	6.40E+02	1.35E+00	1.34E−04	0.00E+00	0.00E+00	1.92E−04	1.22E−03	6.62E−05	0.00E+00	8.28E+02	3.46E+02
17	6.40E+02	1.35E+00	5.13E−03	0.00E+00	0.00E+00	7.38E−03	4.69E−02	2.54E−03	0.00E+00	8.28E+02	3.46E+02
18	5.88E+02	7.48E+00	0.00E+00	0.00E+00	0.00E+00	1.28E−02	4.81E−02	0.00E+00	0.00E+00	1.29E+02	4.37E+02
19	3.75E+02	1.35E+00	5.13E−03	0.00E+00	0.00E+00	7.38E−03	4.69E−02	2.54E−03	0.00E+00	8.28E+02	1.57E+02
20	5.88E+02	7.48E+00	0.00E+00	0.00E+00	0.00E+00	0.00E+00	0.00E+00	0.00E+00	0.00E+00	–	–
21	9.29E+02	7.42E+00	5.51E−03	0.00E+00	0.00E+00	7.27E−03	4.81E−02	2.75E−03	0.00E+00	8.83E+02	7.48E+02
22	5.88E+02	7.48E+00	0.00E+00	0.00E+00	0.00E+00	1.28E−02	4.81E−02	0.00E+00	0.00E+00	1.29E+02	4.37E+02
23	3.64E+02	7.76E+00	0.00E+00	0.00E+00	0.00E+00	0.00E+00	0.00E+00	0.00E+00	0.00E+00	–	–
24	3.64E+02	7.76E+00	0.00E+00	0.00E+00	0.00E+00	0.00E+00	5.62E−05	0.00E+00	2.75E−03	8.20E+05	6.39E+02
25	7.97E+02	7.76E+00	5.50E−03	6.16E−04	9.21E−04	0.00E+00	1.22E−04	2.60E−03	2.75E−03	2.21E+05	1.00E+03
26	1.05E+03	7.48E+00	5.51E−03	0.00E+00	0.00E+00	7.27E−03	4.81E−02	2.75E−03	0.00E+00	8.83E+02	8.63E+02
27	9.29E+02	7.42E+00	5.51E−03	0.00E+00	0.00E+00	7.27E−03	4.81E−02	2.75E−03	0.00E+00	8.83E+02	7.47E+02
28	9.29E+02	7.42E+00	5.51E−03	0.00E+00	0.00E+00	7.27E−03	4.81E−02	2.75E−03	0.00E+00	8.83E+02	7.47E+02
29	8.82E+01	1.32E+00	5.13E−03	0.00E+00	0.00E+00	7.38E−03	4.69E−02	2.54E−03	0.00E+00	8.28E+02	3.07E+01
30	1.01E+02	1.32E+00	1.34E−04	0.00E+00	0.00E+00	1.92E−04	1.22E−03	6.62E−05	0.00E+00	8.28E+02	3.34E+01
31	1.05E+03	7.48E+00	0.00E+00	0.00E+00	0.00E+00	0.00E+00	0.00E+00	0.00E+00	0.00E+00	–	–

temperature-dependent specific heat capacity models, i.e.:

$$\Delta g^0(T) = T\frac{\sum_i \nu_i (g^0_{0,i} - h^0_{0,i})}{T_0} + \sum_i \nu_i h^0_{0,i} + \int_{T_o}^{T} \sum_i \nu_i c_{p,i}\,\mathrm{d}T - T\int_{T_o}^{T} \frac{1}{T}\sum_i \nu_i c_{p,i}\,\mathrm{d}T \quad (3)$$

Of course, when an external load is connected to the cell, its voltage decreases as a consequence of a loss (activation, ohmic, and concentration). These losses or overvoltages are calculated here based on earlier work (e.g., [10]).

3.1.1. Ohmic overvoltage

This loss, due to electron flow through the anode, cathode and interconnections and ion flow though the electrolyte, is evaluated on the basis of Ohm's Law (Eq. (4)). Assuming a series arrangement, the ohmic overvoltage can be calculated by summing over all of the components of the cell (anode, cathode, electrolyte, interconnects). The value of the parameters ξ_i and λ_i, for each component are available in the literature (e.g., [26]):

$$V_{\mathrm{ohm}} = i\sum \delta_i \xi_i \exp\left(\frac{\lambda_i}{T}\right) \quad (4)$$

3.1.2. Activation overvoltage

This type of overvoltage can be calculated on the basis of the Butler–Volmer Eq. (5) and experimental correlations for the anode (Eq. (6)) and cathode (Eq. (7)) exchange current densities [15–17]. In an SOFC, two electrons (n_e) are released for each mole of H_2 reacted (see Eq. (1)). Furthermore, the charge transfer coefficient (α) is considered constant at a value of 0.50 [1–3]:

$$i = i_0\left[\exp\left(\alpha\frac{n_e F}{RT_s}V_{\mathrm{act}}\right) - \exp\left(-(1-\alpha)\frac{n_e F}{RT_s}V_{\mathrm{act}}\right)\right] \quad (5)$$

$$i_{0,\mathrm{anode}} = \gamma_{\mathrm{anode}}\left(\frac{p_{\mathrm{H_2}}}{p_{\mathrm{ref}}}\right)\left(\frac{p_{\mathrm{H_2O}}}{p_{\mathrm{ref}}}\right)\exp\left(\frac{E_{\mathrm{act,anode}}}{RT_s}\right) \quad (6)$$

$$i_{0,\mathrm{cathode}} = \gamma_{\mathrm{cathode}}\left(\frac{p_{\mathrm{O_2}}}{P_{\mathrm{ref}}}\right)^{0.25}\exp\left(-\frac{E_{\mathrm{act,cathode}}}{RT_s}\right) \quad (7)$$

3.1.3. Concentration overvoltage

When reacting hydrogen is not readily replenished from fresh fuel, its partial pressure decreases. The reduction of this partial pressure determines the decrease of cell voltage as a consequence of the shape of the Nernst equation (Eq. (2)). The same phenomenon occurs at the cathode compartment where oxygen is consumed by the cathode electrochemical reaction. The amount of the concentration overvoltage can be calculated taking into account transportation phenomena occurring within the fuel cell, e.g., Eq. (8) [37] which assumes diffusion layers and limits represented by the terms in the brackets, which contain the limiting currents for anode (i_{l,H_2}) and cathode (i_{l,O_2}). Anode and cathode limiting current densities are calculated, respectively, by means of Eqs. (9) and (10), assuming average diffusion coefficients, by neglecting their dependence on temperature, pressure and chemical composition:

$$V_{\mathrm{conc}} = \frac{RT_s}{2F}\log\left[\left(1-\frac{i}{i_{l,\mathrm{H_2}}}\right)\left(1-\frac{i}{i_{l,\mathrm{O_2}}}\right)^{0.5}\right] \quad (8)$$

$$i_{l,\mathrm{H_2}} = 2F\frac{C_{\mathrm{H_2},0}}{1/h_m A} \quad (9a)$$

$$C_{\mathrm{H_2},0} = \frac{y^{\mathrm{anode}}_{\mathrm{H_2}} p_{\mathrm{anode}}}{RT_s} \quad (9b)$$

$$i_{l,\mathrm{O_2}} = 4F\frac{C_{\mathrm{O_2},0}}{1/h_m A} \quad (10a)$$

$$C_{\mathrm{O_2},0} = \frac{y^{\mathrm{cathode}}_{\mathrm{O_2}} p_{\mathrm{cathode}}}{RT_s} \quad (10b)$$

3.1.4. Model validation

All the above mentioned overvoltages are evaluated at the outlet SOFC temperature [14,38]. The overall voltage of the single cell can be calculated as a function of current density, temperatures, pressures, chemical composition and geometric/material characteristics by calculating the difference between the reversible potential and all the overvoltages, i.e.:

$$V = E - V_{\mathrm{ohm}} - V_{\mathrm{concentration}} - V_{\mathrm{activation}} \quad (11)$$

In order to validate the model, the polarization curves generated by the code were compared with experimental ones for different values of operating pressure, temperature, and chemical composition of the inlet streams. Results show that the lumped-parameter model achieves errors lower than 5%, no matter the operating pressure, temperature or inlet chemical composition is considered. For example, Fig. 2 shows the experimental and simulation results at 1000 °C, with inlet composition, pressure and fuel utilization factor as described in [35]. Unfortunately, the data available from Siemens only deals with hydrogen-fuelled SOFCs, so that the validation of the internal reforming process is not yet possible.

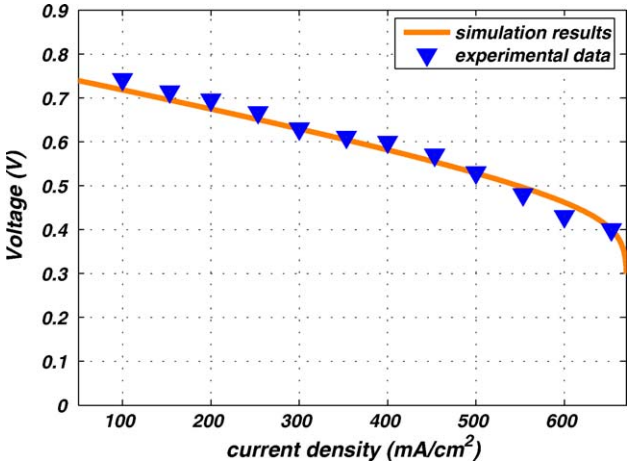

Fig. 2. Fuel cell model validation.

3.2. Turbomachineries

Three turbomachines are included in the plant under study: an air compressor, fuel compressor, and a gas turbine. These devices have been investigated in detail in order to match their requirements with those coming from the fuel cells [38]. Maps, available from the archives of the GSP software and GasTurb, are used, to describe the mass flow rate versus pressure ratio curves for different values of rotor speed. Mass flow rates and rotor speeds are corrected on the basis of their inlet conditions, according to Eqs. (12) [12,28,34]. In the case of the air or fuel compressor, the inlet condition corresponds to the environmental one, whereas the temperature and pressure of the GT inlet stream can vary considerably as a consequence of a change in the design and operating parameters. Consequently, once the GT corrected map is fixed, the uncorrected one changes at each iteration of the procedure, according to the variations of inlet temperature and pressure.

$$\dot{m}_c = \dot{m} \frac{\sqrt{\frac{T_{inlet}}{T_{ref}}}}{\frac{p_{inlet}}{p_{ref}}} \tag{12a}$$

$$N_c = \frac{N}{\sqrt{\frac{T_{inlet}}{T_{ref}}}} \tag{12b}$$

Since no map of commercially available devices matched the values of mass flow rate and pressure ratios required by the components of the plant under investigation, all the maps used in the paper were properly scaled, based on those of the centrifugal compressor ASME 95-GT-79 (Figs. 3 and 4) and the radial turbine NASA-CR-174646 (Fig. 5). Such devices show large ranges for both mass flow rate and pressure ratios, so that a large number of operating points can fall within the feasible region of the maps, as shown in Figs. 3–5.

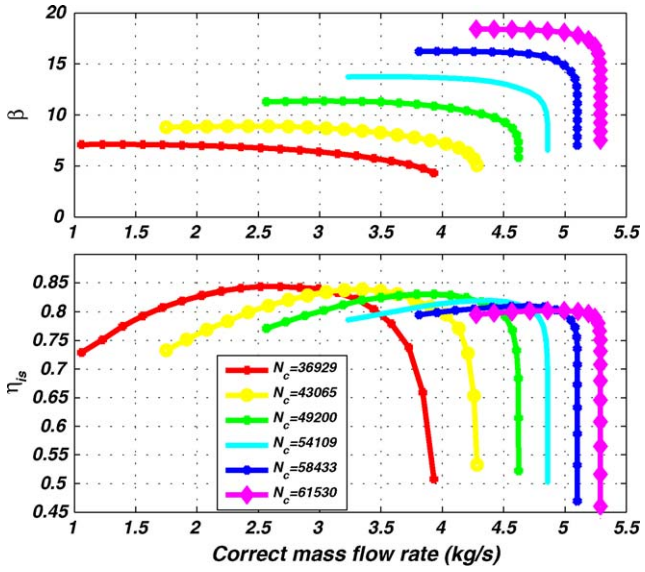

Fig. 3. Air compressor corrected map.

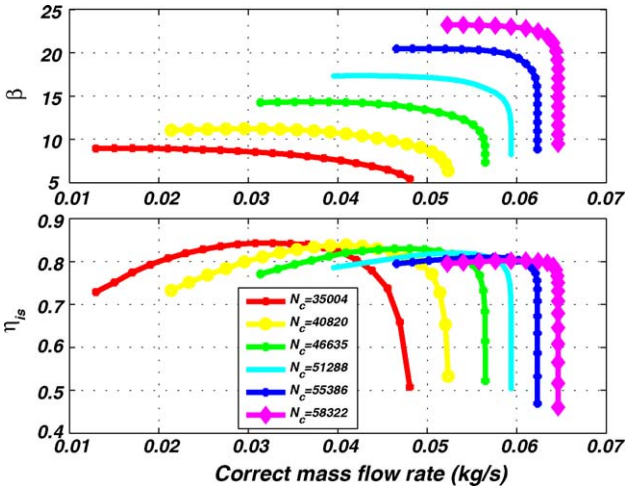

Fig. 4. Fuel compressor corrected map.

Map scaling factors are considered as design decision variables and the code dynamically scales all the maps for each iteration of the optimization procedure.

The air compressor and gas turbine are assumed to be coupled on a single shaft. As a consequence, they must have the same rotor speed. The speed of the fuel compressor can vary independently. The maps are used to calculate isentropic efficiencies and pressure ratios as a function of mass flow rates, rotor speed, and inlet conditions. In particular, a subroutine was developed specifically in order to read maps in the format available from GSP or GasTurb. This subroutine converts this data into a three-dimensional array, i.e. a matrix consisting of isentropic efficiencies, mass flow rates and pressure ratios, for each value of the rotor speed. Finally, the input rotor speed is used to generate the corresponding matrix by means of linear interpolation. Thus, the fixed mass flow rate allows calculation of both pressure ratio and isentropic efficiency by linear interpolation. The outlet conditions of the components are then calculated, as

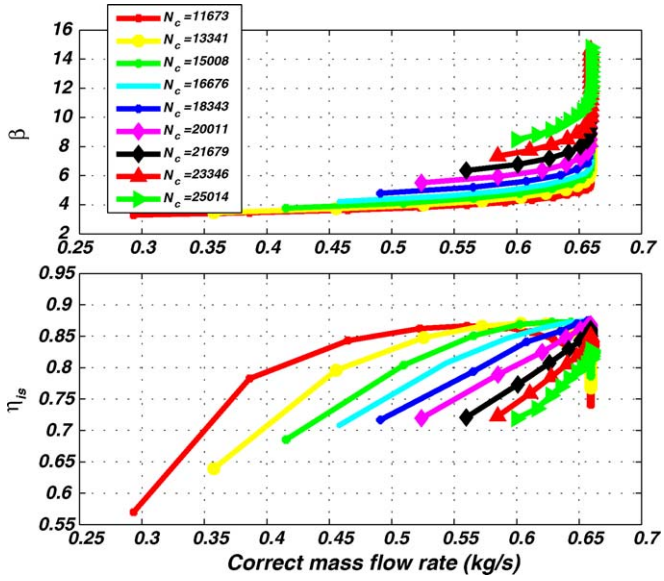

Fig. 5. Gas turbine corrected map.

well as the energy, entropy, and exergy flows. The use of maps dramatically restricts the feasible operating region of the plant. Thus, the solution returned by the simulation code is rejected in the following cases:

- the operating point of a turbomachine falls outside a map;
- the GT outlet pressure calculated is lower than the environmental one;
- the GT mechanical power is lower than that required to move the air com pressor, i.e.: $L_{GT} - L_{AC} \leq 0$.

3.3. Pre-reformer

In theory, SOFCs can be directly fed with natural gas, since the reforming process can be supported inside the stack [1–4,10,14–17,26–29]. In practice, however, a pre-reforming process is always required. In particular, two things must be taken into account, namely:

- the natural gas includes a small fraction of complex hydrocarbons that must be cracked before entering the cell;
- if the cell is directly fed with methane, the bottom of the SOFC tube would not be able to produce any voltage, since there would be no hydrogen available for the electrochemical reaction.

A goal of the study presented here is to quantify the optimum percentage of pre-reformed fuel, since there is a lack of clarity on this issue: in fact, the values available in literature can vary from 30 to 60%. The pre-reformer unit consists of a number of tubes located inside a shell and filled with a particular catalyst [21,22]. The reformate gas flows inside these tubes. Hot gases, coming from the combustor, flow externally, supplying the thermal energy needed to support the process. In fact, the energy provided by the exothermic shift reaction is not sufficient for the endothermic demethanization of the reforming process [21,22]. Furthermore, special attention must be paid to the amount of hot gases mass flow rate required in order to avoid excessive temperature gradients along the cell tubes. If the pre-reforming reactions were not supported by an external hot flow, the pre-reformer's outlet temperature would dramatically decrease. Consequently, the SOFC stack would be fed with an anode inlet stream with a temperature much lower than the equilibrium outlet one, generating unacceptable thermal stresses for the SOFC materials. In order to avoid this circumstance, in the plant under investigation, it is assumed that a controller is installed able to handle the valve, at state point 9, in order to supply the heat flow to the pre-reformer required to match the fixed maximum cell temperature gradient. In order to reach this goal, the required exchange area is usually much higher than the geometric one needed for the reforming reactions. Thus, the exchange area can be increased, with respect to its geometric value, by finning the pre-reformer external area.

In order to simulate this component, the heat-exchange problem must be solved and the chemical composition of the outlet flows must be evaluated as well, taking into account both equilibrium and the kinetics [39–41]. The heat-exchange problem cannot be solved with conventional techniques (log-mean or ϵ-NTU), since chemical reactions occur within the cold fluid. Therefore, an appropriate model is developed based on the differential form of the energy balance equations, integrated along the reformer tubes to calculate the outlet temperatures starting from a set of inlet ones and taking into account the rate at which both the reforming and shift reactions occur in the cold stream. Such model consists of a system of three non-linear algebraic equations, with unknowns the outlet temperatures and heat flow.

The calculation of the rate of reaction is performed on the basis of the following assumptions:

- the shift reaction is equilibrium-controlled;
- for the reforming reaction, both equilibrium and kinetic calculations are performed in order to ascertain the actual state of the reaction[2].

Coefficients of reactions are modeled on the basis of the temperature-dependent Gibbs free energy and specific heats functions [36]. These coefficients are evaluated at the pre-reformer average temperature.

In this paper, the demethanization rate is considered a S/D variable. Thus, its value is fixed during the simulation, allowing the calculation of the rate of the shift reaction on the basis of its chemical equilibrium[3] (Eq. (13)), namely:

$$K_{sh} = \frac{\dot{y}_{H_2}\dot{y}_{CO_2}}{\dot{y}_{H_2O}\dot{x}_{CO}} = \frac{(\dot{n}_{H_2,inlet} + 3\dot{x} + \dot{y} - \dot{z})}{(\dot{n}_{H_2O,inlet} - \dot{x} - \dot{y} + \dot{z})} \frac{(\dot{n}_{CO_2,inlet} + \dot{y})}{(\dot{n}_{CO,inlet} + \dot{x} - \dot{y})} \tag{13}$$

Calculating the value of $\dot{y}$ allows one to evaluate the number of pre-reformer tubes (with their length and diameter fixed) required in order to achieve the fixed demethanization rate, taking into account both the kinetics and equilibrium, i.e.:

$$n_{tubes} = \frac{1}{L_r A_{cr} \rho_B} \int_{\zeta=0}^{\zeta=\dot{x}} \frac{d\zeta}{-\dot{r}_{CH_4}} \tag{14}$$

Finally an equilibrium calculation can be performed, using Eqs. (13) and (15) (with $\dot{z} = 0$), in order to evaluate the demethanization rate. In case this latter value (Eq. (15)) is lower than the above fixed one, the number of tubes are re-calculated with respect to the new value of $\dot{x}$:

$$K_{ref} = \frac{(\dot{n}_{H_2,inlet} + 3\dot{x} + \dot{y} - \dot{z})^3 (\dot{n}_{CO,1} + \dot{x} - \dot{y})}{(\dot{n}_{H_2O,inlet} - \dot{x} - \dot{y} + \dot{z})(\dot{n}_{CH_4,1} - \dot{x})(\dot{n}_{tot,inlet} + 2\dot{x})^2} \times \left(\frac{p}{p^0}\right)^2 \tag{15}$$

[2] In fact, in subsequent work the authors will handle this more straightforwardly by using rate modified expressions for both reactions which incorporate the equilibrium constraints directly into the rate expressions [23,24,42]. Nevertheless, these models require the implementation of a discretization procedure, dramatically increasing computational times. Thus, the authors compared results coming from these two models and verified that, in the case under investigation, the error was lower than 3%.

[3] Obviously, for the pre-reformer simulation $\dot{z} = 0$, since no electrochemical reaction occurs within this component.

The equations for the demethanization rate ($\dot{r}_{CH_4}$) are derived from data available in the literature [21,22,39–41] and can be directly related to the geometric and thermodynamic parameters of the pre-reformer [21,22]. Average temperatures are used to calculate all pre-reformer kinetic and equilibrium properties. These last set of calculations are usually very complex and time-consuming, since a number of non-linear systems of equations must be solved at each iteration. However, it can be simplified by assuming that the demethanization reaction is only ruled by the kinetics. At usual pre-reforming operating temperatures, the methane rate reaction is higher than 90%. In the present work, this value is assumed to range between 20 and 60%: in such a range, the process is ruled by kinetics [1–4].

3.4. Internal reforming

The reformate gas, coming from the pre-reformer, is rich in methane but also consists of hydrogen, carbon monoxide, carbon dioxide, some nitrogen, and steam. Usually, the CO concentration is relatively high, since the conversion rate of the shift reaction is very small and even sometimes negative. As a consequence, it is often necessary to design the fuel cell anode compartment to support both the demethanization and shift reactions within the fuel cell. To do this, a proper catalyst must be used in the region of the SOFC stack where the anode electrochemical reaction takes place. As a consequence, three chemical reactions (demethanization, shift, and electrochemical) must dealt with simultaneously. The unknowns are the methane, carbon monoxide, and hydrogen conversion rates, once all of the geometric parameters are fixed. These variables are calculated on the basis of the shift equilibrium, reforming kinetic/equilibrium, and electrochemical kinetics. From the solution of this strongly non-linear algebraic system of three equations (Eqs. (13), (14) or (15), respectively, for the combined case of kinetic/equilibrium considerations, otherwise Eq. (16)), the chemical compositions at both the anode and cathode outlet can be calculated:

$$U_f = \frac{\dot{z}}{3\dot{x} + \dot{v} + \dot{n}_{H_2,\text{inlet}}} \tag{16}$$

All properties and constants are evaluated at the SOFC outlet equilibrium temperature, since it can be assumed that temperature gradients along the cell radius are negligible as a consequence of the high conductivity and low thickness of materials used in SOFC technology [15,16].

3.5. Combustor, mixers, inverter, electrical generator and heat exchangers

Mixers were modeled on the basis of simple energy and mass balances while the combustor (CO, H_2 and CH_4) reactions are assumed to be driven to completion within the catalytic burner [15,16]. Its outlet chemical composition and energy rates are calculated by using mass and energy balances. Empirical functions were introduced in order to simulate the efficiency of the inverter and the electrical generator as a function of their operational parameters [10]. In order to simulate the heat transfer between the air flowing through the fuel cell air tube and the stream coming from inside the stack (state point 8), a virtual counter-flow tube-in-tube heat exchanger is implemented in the stack [1–4,10,17,26–29]. The heat exchange is simulated on the basis of existing models [15,16], improved to take into account the dependence of the thermo-physical and transport properties on temperature and to include the effects of pressure drops.

Heat transfer coefficients (U) and pressure drops are calculated on the basis of appropriate correlations containing Reynolds, Nusselt and Prandtl numbers [43,44]. These parameters depend both on temperature and pressure, varying along the HE tubes. Consequently, average values are employed, calculated as the mathematical average between inlet and outlet values. Obviously the overall calculation must be performed iteratively, since heat transfer coefficient and pressure drops depend on the unknown outlet temperatures and pressures. For plate-fin heat exchangers, a geometric model is derived from Rancruel [45] and Muñoz [46]. Pressure drops and overall heat exchange coefficients are calculated on the basis of experimental relations given for Colburn and friction factors [45].

Outlet temperatures and pressures must be calculated iteratively by embedded loops and calls to a number of routines for the evaluation of thermo-physical and transport properties. As a consequence, this calculation is very time-consuming. The calculation of the overall heat exchange coefficient for the plate-fin HE strongly depends on its geometry. In particular, both cold- and hot-side heat transfer coefficients must be reduced according to an overall exchange area efficiency. This parameter depends on the geometry of the HE under investigation. The calculation of UA requires evaluation of both h_c and h_h. These coefficients must be evaluated on the basis of the experimental correlation of the Colburn factor, taking into account the minimum flow area, calculated as shown in [45,46]. Finally, the friction factor can be evaluated on the basis of the average Reynolds number and geometric characteristics of the HE, based on the equations in [45,46]. Obviously, the overall calculation must be performed iteratively, since all the average parameters (Reynolds number, Prandtl number, specific heats, etc.) also depend on the as yet unknowns values of outlet temperatures and pressures.

3.6. Solution approach

Due to the complexity of the models developed here and implemented in MATLAB, the calculation of a single operating point is usually a very involved and time-consuming task. Furthermore, whatever optimization approach is used, the search for an optimum set of synthesis/design decision variable values requires the calculation of a very high number of possible syntheses/designs for the plant. Thus, a great deal of effort has been spent by the authors to speed-up the calculation procedure by lightening the number of sub-functions, replacing the graphic interface, and introducing more efficient algorithms than available in MATLAB for the solution of integrals and non-linear systems of equations. This effort has resulted in a reduction by a factor of 4 of the computational time. In addition, since the code is written in MATLAB, which is not designed for the solution of strongly non-linear systems, the code has been written to the greatest extent possible using a sequential logic, which

avoids having to solve a system or a set of systems of equations simultaneously. Nonetheless, in certain cases this is unavoidable and an iterative procedure is needed for some subsystems of the plant. In particular, four main nested loops are introduced, respectively, to calculate in the following:

(1) the chemical composition at state point 3;
(2) the pressure and temperature at the outlet of the SOFC stack;
(3) the temperature, pressure, and chemical composition at the outlet of the GT;
(4) the fuel flow rate.

Since the solutions of the pre-reformer and stack subsystems require knowledge of all inputs, including the chemical composition at state point 3 and the latter depends on the characteristics and operating conditions of the stack and the GT, a guess value for chemical composition at state point 3 is used, starting from the value of the mass flow rate at state point 5. In other words, the re-circulation ratio is calculated in order to match the value of the steam-to-carbon ratio required to avoid carbon deposition in the anode compartment of the fuel cell. The mixer, pre-reformer, and stack are then solved followed by the anode outlet chemical composition. This is then compared with the initial guess and the iteration proceeds until the convergence criterion on the partial pressures of all the chemical constituents is satisfied.

The preceding iterative calculation requires the temperature of the stack, which must be iteratively calculated by the second loop mentioned above. Furthermore, both the preheating heat exchangers require the chemical composition, temperature, and pressure at state point 10. These can be calculated iteratively, by means of the third loop mentioned above. Finally, the fuel flow rate is iteratively calculated until the required net electrical power is achieved.

4. Cost model

In order to perform a thermoeconomic analysis and optimization, the capital cost must be estimated, for each component of the plant, at any given set of values assumed by the synthesis/design decision variables. For the turbomachinery, the capital cost is usually evaluated on the basis of the maximum power produced. In particular, for the gas turbine, the cost function proposed by Massardo et al. [47] is used, i.e.:

$$C_{\mathrm{GT}} = (-98.328 \ln(\dot{P}_{\mathrm{GT}}) + 1318.5)\dot{P}_{\mathrm{GT}} \tag{17}$$

For the centrifugal compressors, the capital costs are calculated by interpolating data from manufacturers as a function of the maximum power required and using information provided in recent papers [48,49]. On this basis, the cost is given by

$$C_{\mathrm{compressor}} = 91562\left(\frac{\dot{P}_{\mathrm{compressor}}}{445}\right)^{0.67} \tag{18}$$

The estimated capital costs of the compact heat exchangers is related to their mass which can be evaluated on the basis of the geometric model. Thus:

$$C_{\mathrm{HE}} = 111.6(m_{\mathrm{HE}})^{0.95} \tag{19}$$

For the counter-flow heat exchanger, the capital cost is determined on the basis of literature data [50] such that:

$$C_{\mathrm{HEC}} = 130\left(\frac{A_{\mathrm{HE}}}{0.093}\right)^{0.78} \tag{20}$$

The cost of the SOFC stack is not calculated at present market values, since the technology is still sometime away from full commercialization. Thus, the cost is estimated with reference to market studies in which the expected cost for the case of a significant increase in production volumes is assumed. A detailed work performed by [51] relates the SOFC capital cost to the active area and the operating temperature. Furthermore, the electric energy produced by the SOFC must be filtered by an inverter, whose cost is not negligible and should, therefore, be taken into account. This cost depends primarily on the net power production of the stack. Thus, for both of these costs, the following expressions are used:

$$C_{\mathrm{SOFC}} = (n_{\mathrm{cells}}\pi D_{\mathrm{cell}} L_{\mathrm{cell}})(2.96 t_{\mathrm{cell}} - 1907) \tag{21}$$

$$C_{\mathrm{inverter}} = 10^5\left(\frac{\dot{P}_{\mathrm{cell}}}{500}\right)^{0.70} \tag{22}$$

The SOFC system also consists of a pre-reformer, whose cost is calculated on the basis of its catalyst volume and the finned exchange area [21,22,50] which is related to the number, diameter, and length of tubes. Thus, based on these references and updating the functions with literature data, the following cost function is

$$C_{\mathrm{PR}} = 130\left(\frac{A_{\mathrm{PR,fin}}}{0.093}\right)^{0.78} + 3240(V_{\mathrm{PR}})^{0.4} + 21280.5 V_{\mathrm{PR}} \tag{23}$$

Finally, the capital costs for auxiliary devices such as the combustor, mixers, and by-pass valves are calculated as a fixed percentage (10%) of the stack cost while the counter-flow heat exchanger cost is given by a cost function found in [51]:

$$C_{\mathrm{aux,SOFC}} = 0.10 C_{\mathrm{SOFC}} \tag{24}$$

The overall life cycle cost for owning and operating the plant is assumed as the objective function to be minimized. It is defined as the sum of the fuel and capital costs evaluated on a yearly basis. The following assumptions are made: 87,600 operating hours over the lifetime of the plant; an amortization rate of 5%. The cost avoided through the use of waste heat (Q_{rec}) is also considered, assuming a reference efficiency for conventional furnaces (η_{c}) of 90%. Maintenance costs are not included into the objective function since they are assumed independent of the S/D variables. Thus, the objective function (OF) to be minimized is as follows:

$$\mathrm{OF} = \zeta \sum_i C_i + c_{\mathrm{fuel}} \dot{V}_{\mathrm{fuel}}(N_{\mathrm{h}}) - \frac{c_{\mathrm{fuel}} \dot{Q}_{\mathrm{rec}}(N_{\mathrm{h}})}{\mathrm{LHV}(\eta_{\mathrm{c}})} \tag{25}$$

with $\zeta = 0.12951\ \mathrm{yr}^{-1}$, $N_{\mathrm{h}} = 8760\ \mathrm{h\ yr}^{-1}$, $\mathrm{LEV} = 9.59\ \mathrm{kWh\ N}^{-1}\ \mathrm{m}^{-3}$.

5. Optimization strategy

The optimization of the hybrid plant investigated is a very complex problem due to the non-linearity of the models, the high degree of coupling between components, the high number of synthesis/design decision variables, and the continuous and discrete nature of these variables. Furthermore, the performance maps for the compressors and turbine, introduced to develop a more realistic model, dramatically restrict the region of feasible solutions, leading to a large number of simulations with infeasible operating points. To more effectively deal with these difficulties, a genetic algorithm (GA) is used [30]. Such an approach is very calculation intensive and, unlike with a gradient-based approach, is unable to mathematically establish a Kuhn–Tucker point, since it is a heuristic method. This can be circumvented by coupling the two types of optimization approaches together [18,20,21,23,24,45,46], with the GA doing the general search of the optimization solution space and the gradient method helping narrow the search to a particular Kuhn–Tucker point or boundary. This is not done here, due to software integration issues which have yet to be resolved. Nonetheless, the GA in and of itself is a very powerful tool to handle strongly non-linear, non-continuous, mixed integer optimization problems and is, thus, used here. Finally, the initial population for the GA is set at four times the number of decision variables while the number of generations is set to a very high value (700). The GA is stopped when no improvements of the objective function for a number of generations is observed.

6. Case study, results and discussion

This single-level optimization strategy was run on a PIV 3.0 GHz, 1 Gb RAM PC and required more than a month of continuous execution to arrive at a single optimum solution. Usually, more than 250 generations were required to get close to the optimum design configuration. As mentioned above, the values for the fixed parameters in this case study are summarized in Table 1 while Table 2 lists the synthesis/design decision variables, their initial values, their optimum values (w.r.t. c_{fuel} varying from 0.10 to 0.30 US$ $\text{N}^{-1}\,\text{m}^{-3}$, with a step of 0.05 US$ $\text{N}^{-1}\,\text{m}^{-3}$), and their ranges. The optimization was performed with different values of the cost of the fuel in order to take into account the sensitivity of the model to varying such a parameter. Tables 3 and 4 summarize the most important thermodynamic information about plant performance for the optimum syntheses/designs and the initial, respectively (case 3: $c_{\text{fuel}} = 0.20$ US$ $\text{N}^{-1}\,\text{m}^{-3}$). Furthermore, by comparing the optimum and initial design conditions, it can be seen that the initial configuration has been dramatically modified by the optimizer, resulting in an improvement of the objective function usually higher than 20% (see Fig. 6). This is a very remarkable result, if one takes into account how small the region of feasible solutions is for the plant investigated.

6.1. Optimized syntheses/designs

The optimization made some important adjustments to the heat exchanger and turbomachinery syntheses/designs. The latter, in particular, is due to the complex relationship existing between the turbomachinery and the fuel cell stack. Initial maps of the turbomachinery are strongly scaled, since the optimum scaling factors are found to be close to the boundary of the optimal search region (see parameters 3, 4, 44, 45, 46 and 47 in Table 2). In fact, a special adjustment is made to the fuel compressor map, since a non-optimal design of this component could result in remarkable inefficiencies due to throttling of the fuel before entering the stack. Conversely, the optimizer does not significantly change the value initially assumed for the rotor speed. This result depends on the shape of the turbomachinery maps, since their design point is set very close to the minimum rotor speed. For higher rotor speeds, the code produces infeasible points or very low values of the isentropic efficiency. Table 4 (see parameters 41 and 42) also shows that both optimum by-pass mass flow rates are very close to the initial values. This implies that the optimum configuration corresponds to by-pass valves (state points 23 and 31) almost completely closed. Obviously, during part-load operation the management of such by-pass valves will be very useful for controlling both stack and GT inlet temperatures.

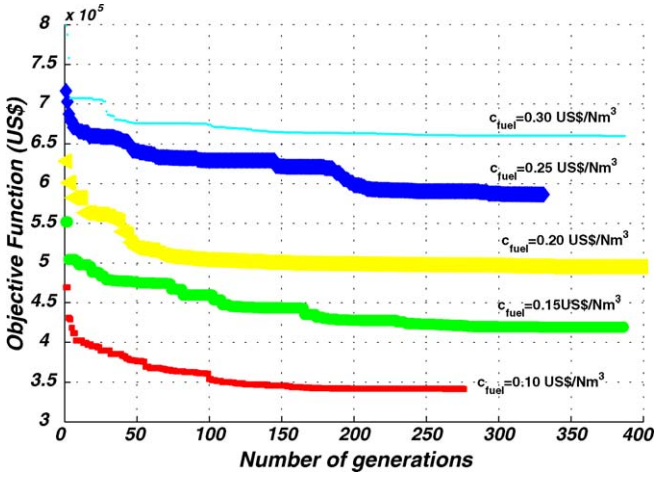

Fig. 6. GA optimization procedure.

SOFC geometric parameters are also remarkably changed. The initial synthesis/design corresponds to a very low value of the current density at the design point. This allows the stack to achieve a very high potential but results in higher capital costs, since a higher number of tubes with greater length and diameters are required. The optimization procedure dramatically reduces the cell active area by decreasing the number, diameter, and length of tubes. Such optimum values are very slightly dependent on the cost of fuel, as shown in Table 2.

The optimum demethanization rate in the pre-reformer is also very low. High values of the demethanization rates are not useful, since the cell can support almost the entire reforming process internally. Higher values of the area and volume used for pre-reforming imply higher costs, which can be avoided because the same process can be realized within the fuel cell stack.

Table 2 also shows the optimum value of the geometric variables of the compact heat exchangers. No useful data in the literature for initial values for these variables was available. As

Table 4
Thermodynamic properties of the optimum configuration ($c_{fuel} = 0.20$ US$ N^{-1} m^{-3})

State point	t	p	$\dot{n}_{H_2O}$	$\dot{n}_{CO}$	$\dot{n}_{H_2}$	$\dot{n}_{O_2}$	$\dot{n}_{N_2}$	$\dot{n}_{CO_2}$	$\dot{n}_{CH_4}$	ex_{ch}	ex_{ph}
1	3.17E+02	8.31E+00	0.00E+00	0.00E+00	0.00E+00	0.00E+00	5.61E−05	0.00E+00	2.75E−03	8.20E+05	5.12E+02
2	8.19E+02	8.31E+00	4.80E−03	1.33E−03	3.14E−03	0.00E+00	1.22E−04	2.64E−03	1.99E−03	2.02E+05	1.10E+03
3	8.99E+02	8.31E+00	1.02E−02	9.66E−04	1.72E−03	0.00E+00	1.22E−04	5.00E−03	6.23E−08	4.71E+04	9.98E+02
4	8.99E+02	8.31E+00	4.71E−03	4.45E−04	7.94E−04	0.00E+00	5.61E−05	2.30E−03	2.87E−08	4.71E+04	9.98E+02
5	8.99E+02	8.31E+00	5.50E−03	5.21E−04	9.28E−04	0.00E+00	6.56E−05	2.69E−03	3.36E−08	4.71E+04	9.98E+02
6	5.33E+02	7.70E+00	0.00E+00	0.00E+00	0.00E+00	1.36E−02	5.11E−02	0.00E+00	0.00E+00	1.29E+02	4.01E+02
7	8.99E+02	7.70E+00	0.00E+00	0.00E+00	0.00E+00	8.70E−03	5.11E−02	0.00E+00	0.00E+00	1.65E+02	6.92E+02
8	1.03E+03	7.70E+00	5.50E−03	0.00E+00	0.00E+00	8.08E−03	5.11E−02	2.75E−03	0.00E+00	8.17E+02	8.50E+02
9	9.80E+02	7.70E+00	5.50E−03	0.00E+00	0.00E+00	8.08E−03	5.11E−02	2.75E−03	0.00E+00	8.17E+02	7.975+02
10	5.13E+02	1.07E+00	5.50E−0S	0.00E+00	0.00E+00	8.08E−03	5.11E−02	2.75E−03	0.00E+00	8.17E+02	2.28E+02
11	2.88E+02	1.06E+00	1.34E−04	0.00E+00	0.00E+00	1.97E−04	1.24E−03	6.69E−05	0.00E+00	8.17E+02	8.69E+01
12	2.50E+01	1.00E+00	0.00E+00	0.00E+00	0.00E+00	1.36E−02	5.11E−02	0.00E+00	0.00E+00	1.29E+02	0.00E+00
13	2.96E+02	7.71E+00	0.00E+00	0.00E+00	0.00E+00	1.36E−02	5.11E−02	0.00E+00	0.00E+00	1.29E+02	2.57E+02
14	2.50E+01	1.00E+00	0.00E+00	0.00E+00	0.00E+00	0.00E+00	5.61E−05	0.00E+00	2.75E−03	8.20E+05	0.00E+00
15	2.32E+02	8.31E+00	0.00E+00	0.00E+00	0.00E+00	0.00E+00	5.61E−05	0.00E+00	2.75E−03	8.20E+05	4.54E+02
16	5.14E+02	1.07E+00	1.34E−04	0.00E+00	0.00E+00	1.97E−04	1.24E−03	6.69E−05	0.00E+00	8.17E+02	2.29E+02
17	5.14E+02	1.07E+00	5.37E−03	0.00E+00	0.00E+00	7.88E−03	4.99E−02	2.68E−03	0.00E+00	8.17E+02	2.29E+02
18	4.68E+02	7.70E+00	0.00E+00	0.00E+00	0.00E+00	1.36E−02	5.11E−02	0.00E+00	0.00E+00	1.29E+02	3.57E+02
19	3.52E+02	1.05E+00	5.37E−03	0.00E+00	0.00E+00	7.88E−03	4.99E−02	2.68E−03	0.00E+00	8.17E+02	1.21E+02
20	4.68E+02	7.70E+00	0.00E+00	0.00E+00	0.00E+00	0.00E+00	0.00E+00	0.00E+00	0.00E+00	–	–
21	8.91E+02	7.69E+00	5.50E−03	0.00E+00	0.00E+00	8.08E−03	5.11E−02	2.75E−03	0.00E+00	8.17E+02	7.13E+02
22	4.68E+02	7.70E+00	0.00E+00	0.00E+00	0.00E+00	1.36E−02	5.11E−02	0.00E+00	0.00E+00	1.29E+02	3.57E+02
23	3.17E+02	8.31E+00	0.00E+00	0.00E+00	0.00E+00	0.00E+00	2.75E−08	0.00E+00	1.35E−06	8.20E+05	5.72E+02
24	3.17E+02	8.31E+00	0.00E+00	0.00E+00	0.00E+00	0.00E+00	5.61E−05	0.00E+00	2.75E−03	8.205+05	5.72E+02
25	7.30E+02	8.31E+00	5.50E−03	5.21E−04	9.28E−04	0.00E+00	1.22E−04	2.69E−03	2.75E−03	2.19E+05	9.02E+02
26	9.80E+02	7.70E+00	5.50E−03	0.00E+00	0.00E+00	8.08E−03	5.11E−02	2.75E−03	0.00E+00	8.17E+02	7.975+02
27	8.91E+02	7.69E+00	5.50E−03	0.00E+00	0.00E+00	8.08E−03	5.11E−02	2.75E−03	0.00E+00	8.17E+02	7.13E+02
28	8.91E+02	7.69E+00	5.50E−03	0.00E+00	0.00E+00	8.08E−03	5.11E−02	2.75E−03	0.00E+00	8.17E+02	7.13E+02
29	6.31E+01	1.03E+00	5.37E−03	0.00E+00	0.00E+00	7.88E−03	4.99E−02	2.68E−03	0.00E+00	8.17E+02	5.16E+00
30	9.55E+01	1.04E+00	1.34E−04	0.00E+00	0.00E+00	1.97E−04	1.24E−03	6.69E−05	0.00E+00	8.17E+02	1.14E+01
31	9.80E+02	7.705+00	0.00E+00	0.00E+00	0.00E+00	0.00E+00	0.00E+00	0.00E+00	0.00E+00	–	–

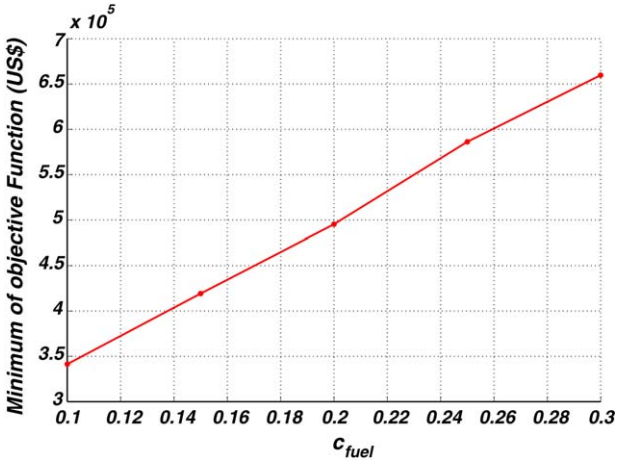

Fig. 7. Minimum value of the objective function.

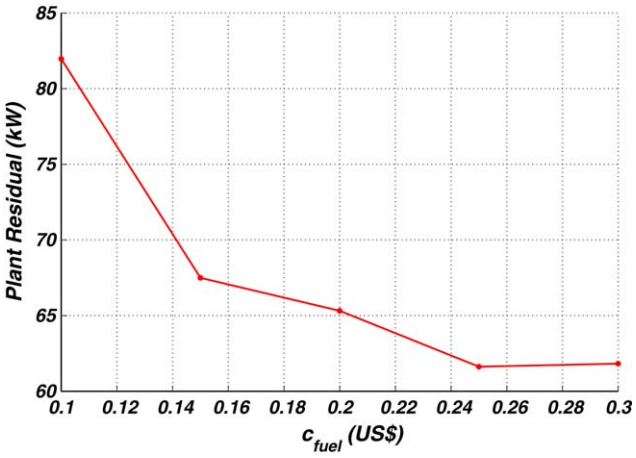

Fig. 9. Exergy losses at the optimum point (kW).

can be seen from the table, the initial values are very far from the optimum. Furthermore, the optimum value of the first design variable listed in Table 2 ($f_d = \dot{m}_{17}(\dot{m}_{12} + \dot{m}_{14})/(\dot{m}_{10}\dot{m}_{12})$) is very close to 1, as expected. In fact, the nominal mass flow rate was set in order to have both preheaters "balanced".

6.2. Optimized costs, energy and exergy flows

Fig. 7 shows that the optimum values of the objective function are linearly dependent on the cost of fuel. Obviously, the higher the cost of the fuel is, the higher the overall efficiency of the plant will be (see Fig. 8). This increase is mainly due to the higher value of plant thermal efficiency. In fact, plant electrical efficiency does not show remarkable changes with respect to the value corresponding to the initial value (67.9%). Increasing the thermal efficiency results in larger savings in terms of heating avoided costs. In addition, with increasing cost of fuel, the exergy losses (exergy flows at state points 29 and 30) at the optimum point remarkably decrease (Fig. 9). On the other hand, plant optimum electrical efficiency is almost constant (see Fig. 8), showing a very slight dependence on the cost of fuel. Consequently, whatever cost of fuel is considered, once the plant electrical power is fixed, the optimum amount of fuel required by the plant is almost constant.

The simulation code returns a remarkably high value of the net electrical efficiency since it is based on a single-point steady-state design. Obviously the same plant would have a somewhat lower average efficiency if the transient behavior had been taken into account during the optimization process [23,24,42]. Figs. 10–13, respectively, show thermal and mechanical flows, exergy destruction rates, and component costs determined for the initial synthesis/design, and for the optimized configurations varying the cost of the fuel. For the initial synthesis/design, the capital cost is mainly due to the fuel cell stack, as expected. The costs of the turbomachinery are much higher than those for the heat exchangers, especially for the GT. The exergy destruction rate is primarily due to the combustor, the SOFC, the GT, and the HE4. The inefficiency of the turbomachinery (GT and compressors) is mainly caused by a non-ideal coupling so that at the initial design point, the turbomachinery does not achieve its highest values of isentropic efficiency. Finally, a significant irreversibility is due to the heat transfer within the gas-to-water

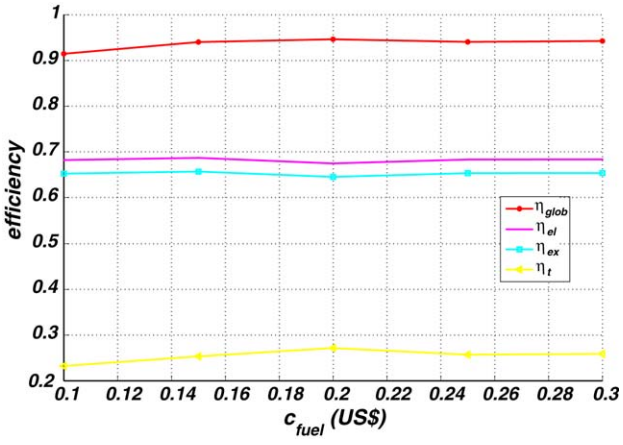

Fig. 8. Optimum efficiencies.

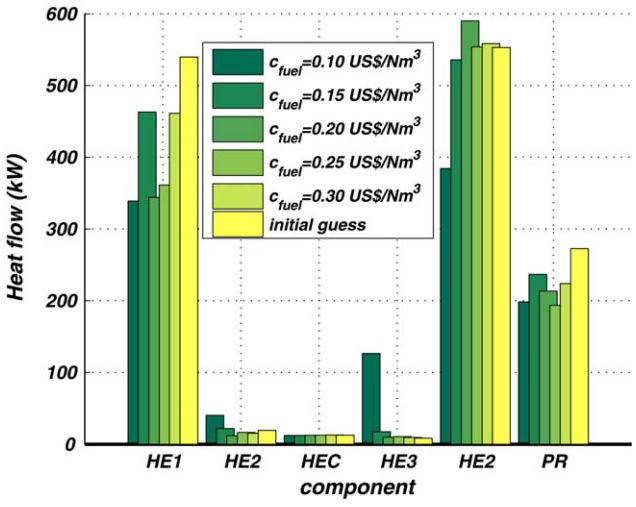

Fig. 10. Thermal flow rates in the heat exchangers: initial and optimum values (kW).

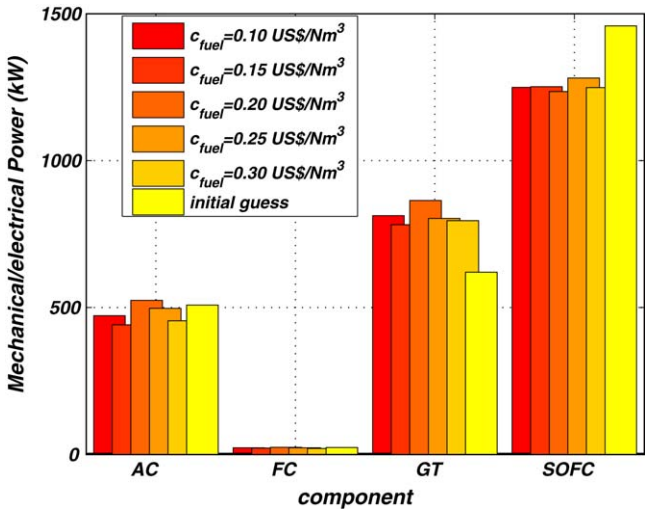

Fig. 11. Mechanical and electrical power: initial and optimum values (kW).

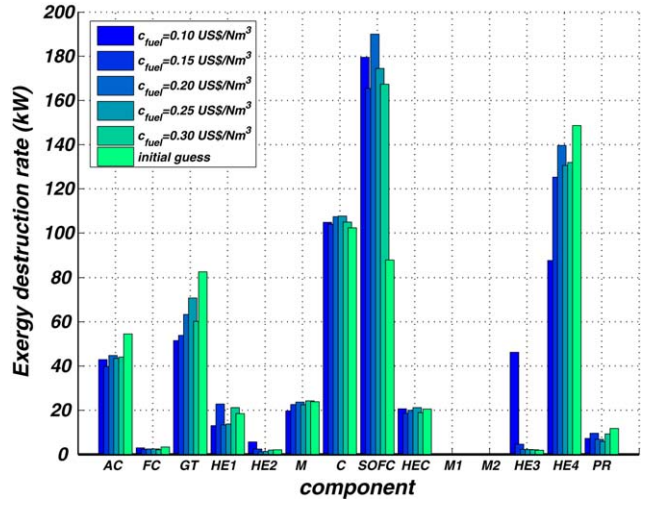

Fig. 12. Exergy destruction rate for the various components at the optimum point (kW).

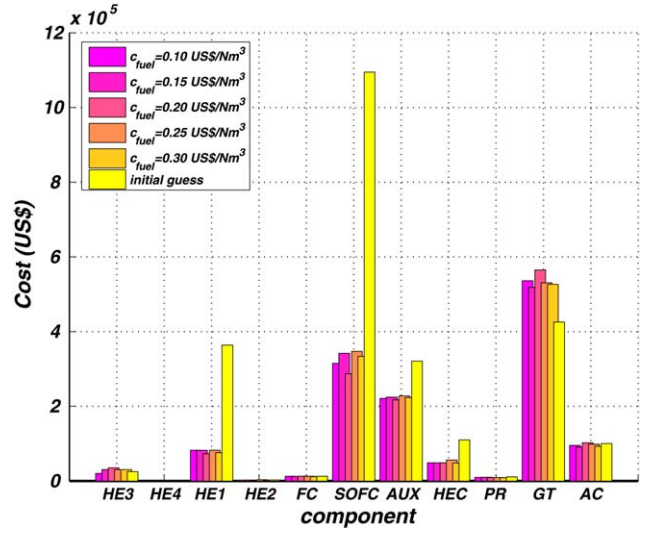

Fig. 13. Capital costs of the components: initial and optimum values (US$).

heat exchangers, caused by very high temperature differences. After optimization, the role of the stack is reduced, since there is a greater share of the power required and produced by the turbomachinery. As a consequence, the SOFC capital cost decreases and that of the turbomachinery increases. Furthermore, the cell inefficiency remarkably increases, due to the reduction of the active area. This loss in efficiency is compensated by a lower investment cost, leading to a better value of the system-level objective.

As mentioned above, increasing the cost of fuel, plant thermal efficiency increases. In fact, as shown in Fig. 10, the higher the cost of fuel is, the higher the heat flow exchanged in the HE4 is. Consequently, better values of the objective function can be achieved. Similarly, increasing c_{fuel}, results in remarkably higher values of HE1. Conversely, Fig. 11 shows the mechanical/electrical power is slightly dependent on the fuel cost. This is mainly due to the above mentioned shape of the optimum electrical efficiency function. Thus, exergy destruction rates are sensitive to c_{fuel} mainly in the heat exchangers, as shown in Fig. 12. This figure also shows that the higher c_{fuel} is, the lower the exergy destruction rates produced by the GT and SOFC are.

7. Conclusions

The optimization described in this paper shows that the design of a hybrid SOFC–GT power plant must focus on all the components of the system, paying special attention to their coupling. The optimization procedure finds a system configuration with much lower capital costs than that of the initial configuration yet with similar values of the net electrical efficiencies. In addition, the optimal results show that the SOFC is not necessarily the most expensive component of the plant. Furthermore, to achieve the high efficiency and low costs the optimization procedure provided optimal values for all 48 S/D variables of which some of the more important are the pre-reforming ratio, heat exchange area and SOFC active area. The typical mistake of optimizing the stack as an isolated device should be avoided, since inefficiencies in the turbomachinery and in the balance of plant can be significant. In addition, the perspective of a full commercialization of solid oxide fuel cells is expected to lower their capital costs so that this component will not necessarily be the most expensive in the plant. However, as useful as the results from this optimization are with respect to the optimal synthesis/design of this plant, they will be incomplete until off-design conditions are also taken into account during the optimization process. As indicated earlier, this is the subject of future papers.

Acknowledgements

Financial support by the CNR (National Research Council) and the University of Naples Federico II are gratefully acknowledged.

References

[1] S.C. Singhal, K. Kendall, High Temperature Solid Oxide Fuel Cells, Elsevier, 2003.

[2] J. Larminie, A. Dicks, Fuel Cell System Explained, John Wiley and Sons Ltd., 2004.
[3] T.G. Benjamin, E.H. Camera, L.G. Marianowski, Handbook of Fuel Cell Performance, Institute of Gas Technology, 1995.
[4] Fuel Cell Handbook, 6th ed., U.S. Department of Energy, 2002.
[5] Fuel Cell Technology Handbook, Gregors Hoogers/CRC Press/SAE International, 2002, Hardbound.
[6] J. Palsson, A. Selimovic, L. Sjunnesson, Combined solid oxide fuel cell and gas turbine systems for efficient power and heat generation, J. Power Sources 86 (2000) 442–448.
[7] S. Kimijima, N. Kasagi, Performance evaluation of gas turbine–fuel cell hybrid micro generation system, in: Proceedings of ASMETURBO EXPO 2002, June 3–6, Amsterdam, The Netherlands, 2002.
[8] B.H. Bae, J.L. Sohn, S.T. Ro, Thermodynamic modeling and performance analysis of a power generation system based on the solid oxide fuel cell, in: Proceedings of ASME Conference on Fuel Cell Science, Engineering and Technology, April 21–23, Rochester, NY, USA, 2003.
[9] Y. Inui, S. Yanagisawa, T. Ispida, Proposal of high performance SOFC combined power generation system with carbon dioxide recovery, Energy Convers. Manage. 44 (2003) 597–609.
[10] Campanari, S., Power plants based on solid oxide fuel cells combined with gas turbine cycles, Ph.D. Dissertation, Politecnico di Milano, Milano, 1998.
[11] K.W. Bedringas, I.S. Ertesvag, Exergy analysis of solid oxide fuel cell systems, Energy: Int. J. 22 (1997) 403–412.
[12] W.R. Dunbar, N. Lior, R. Gaggioli, Combining fuel cells with fuel-fired power plants for improved exergy efficiency, Energy: Int. J. 16 (10) (1991) 1259–1274.
[13] W.R. Dunbar, N. Lior, R. Gaggioli, The effect of the fuel-cell unit size on the efficiency of a fuel-cell-topped Rankine Cycle, ASME J. Energy Resour. Technol. 115 (1993) 105–107.
[14] S.H. Chan, C.F. Low, O.L. Ding, Energy and exergy analysis of a simple solid-oxide fuel cell power system, J. Power Sources 103 (2002) 188–200.
[15] F. Calise, M. Dentice d'Accadia, A. Palombo, L. Vanoli, Simulation and exergy analysis of a hybrid SOFC–gas turbine system, part I: description of the model, in: Proceedings of the 17th International Conference on Efficiency. Costs. Optimization. Simulation and Environmental Impact of Energy and Process Systems, Gunajuato, Mexico, July 7–9, 2004.
[16] F. Calise, M. Dentice d'Accadia, A. Palombo, L. Vanoli, Simulation and exergy analysis of a hybrid SOFC–gas turbine system, part II: results and discussion, in: Proceedings of the 17th International Conference on Efficiency. Costs. Optimization. Simulation and Environmental Impact of Energy and Process Systems, Gunajuato, Mexico, July 7–9, 2004.
[17] F. Calise, M. Dentice d'Accadia, A. Palombo, L. Vanoli, R. Vanoli, Modelling, simulation and exergy analysis of a hybrid SOFC–gas turbine system, in: Proceedings of the Third International Symposium on Energy and Environment, Sorrento, 30 September–2 October, 2004.
[18] J.R. Muñoz, M.R. von Spakovsky, The use of decomposition approach for the large scale synthesis/design optimization of highly coupled, highly dynamic energy systems, Int. J. Appl. Thermodyn. 4 (1) (2001).
[19] C.A. Frangopoulos, M.R. von Spakovsky, E. Sciubba, A brief review of methods for the design and synthesis optimization of energy systems, in: ICAT, vol. 5, no.4, Istanbul, Turkey, December, Int. J. Appl. Thermodyn. (2002).
[20] D.F. Rancruel, M.R. von Spakovsky, Decomposition with thermoeconomic isolation applied to the optimal synthesis/design of an advanced fighter aircraft system, in: ICAT, vol. 6, no. 3, Istanbul, Turkey, September, Int. J. Thermodyn. (2003).
[21] N. Georgopoulos, Application of a decomposition strategy to the optimal synthesis/design and operation of a fuel cell based total energy system, M.S. thesis, advisor: M. R. von Spakovsky, Virginia Polytechnic Institute and State University, Blacksburg, VA, 2001.
[22] B. Oyarzabal, Application of a decomposition strategy to the optimal synthesis/design of a fuel cell sub-system, M.S. thesis, advisor: M.R. von Spakovsky, Virginia Polytechnic Institute and State University, Blacksburg, VA, 2001.
[23] D.F. Rancruel, Dynamic synthesis/design and operational/control optimization approach applied to a solid oxide fuel cell based auxiliary power unit under transient conditions, Ph.D. Dissertation, Advisor: M.R. von Spakovsky, Virginia Polytechnic Institute and State University, Blacksburg, VA, 2005.
[24] D.F. Rancruel, M.R. von Spakovsky, Development and application of a dynamic decomposition strategy for the optimal synthesis/design and operational/control of a SOFC based APU under transient conditions, Proceedings of the International Mechanical Engineering Congress and Exposition—IMECE'2005, ASME Paper No. 82986, New York, NY, November, 2005.
[25] http://www.fuelcells.org.
[26] P. Costamagna, L. Magistri, A.F. Massardo, Design and part-load performance of a hybrid system based on a solid oxide fuel cell reactor and a micro gas turbine, J. Power Sources 96 (2001) 352–368.
[27] S. Campanari, Carbon dioxide separation from high temperature power plants, J. Power Sources 112 (2002) 273–289.
[28] S. Campanari, Full load and part load performance prediction for integrated SOFC and microturbine systems, J. Power Sources 96 (2001) 352–368.
[29] S. Campanari, Thermodynamic model and parametric analysis of a tubular SOFC module, J. Power Sources 92 (2001) 26–34.
[30] MOOLENI Geneticalgorithm Software. LENI, Ecole Polytechnique Federate de Lausanne, Lausanne, Switzerland, 2004.
[31] S. Bellavia, M. Macconi, B. Morini, An affine scaling trust region method approach to bound-constrained nonlinear systems, Appl. Numer. Math. 44 (2003) 257–280.
[32] S. Bellavia, M. Macconi, B. Morini, STRSCNE: a scaled trust region solver for constrained nonlinear equations, Technical Report, 2002.
[33] http://www.iapws.org/newform.htm.
[34] Chemical Properties Handbook, McGraw Hill, 1999, pp. 531–556.
[35] S.C. Singhal, Recent progress in tubular solid oxide fuel cell technology, in: Proceedings of the Fifth International Symposium on Solid Oxide Fuel Cells, 1997.
[36] E.P. Giyftopoulos, G.P. Beretta, Thermodynamics: Foundations and Applications, Macmillan, New York, 1991.
[37] F. Marechal, D. Favrat, F. Palazzi, J. Godat, Thermoeconomic modeling and optimization of fuel cell systems, in: Proceedings of the Fuel Cell Research Symposium, ETH Zrich, March, 2004.
[38] S.H. Chan, H.K. Ho, Y. Tian, Modeling for part load operation of solid oxide fuel cell–gas turbine hybrid power plant, J. Power Sources 114 (2003) 213–227.
[39] M. Zanfir, A. Gavrilidis, Catalytic combustion assisted methane steam reforming in a catalytic plate reactor, Chem. Eng. Sci. 58 (2003) 3947–3960.
[40] F. Gallucci, L. Paturzo, A. Basile, A simulation study of the steam reforming of methane in a dense tubular membrane reactor, Int. J. Hydrogen Energy 29 (2004) 611–617.
[41] J. Xu, G.F. Froment, Methane–steam reforming: methanation and water–gas shift. I. Intrinsic kinetics, AlXhE J. (1989).
[42] D.F. Rancruel, M.R. von Spakovsky, Investigation of the control strategy development using an integrated model of a SOFC based APU under transient conditions, Proceedings of the International Mechanical Engineering Congress and Exposition—IMECE'2004, ASME Paper No. 62372, New York, NY, November, 2004.
[43] S. Kakac, H. Liu, Heat Exchanger Selection, Rating, and Thermal Design, CRC Press, Boca Raton, FL, 1998.
[44] W.M. Kays, A.L. London, Compact Heat Exchangers, 3rd ed., Krieger Publishing Company, Florida, 1998.
[45] D.F. Rancruel, A decomposition strategy based on thermoeconomic isolation applied to the optimal synthesis/design and operation of an advanced fighter aircraft system, M.S. Thesis, Advisor: M.R. von Spakovsky, Virginia Polytechnic Institute and State University, Blacksburg, VA, 2003.
[46] J.R. Muñoz, Optimization strategies for the synthesis/design of highly coupled, highly dynamic energy systems, Ph.D. Dissertation, Advisor: M.R. von Spakovsky, Virginia Polytechnic Institute and State University, Blacksburg, VA, 2000.
[47] Traverso, A., Massardo, A., Logorio, G., Cazzola, W., 2004. WIDGET-TEMP: a novel web-based approach for thermoeco-nomic analysis and optimization of conventional and innovative cycles, ASME Paper 2004-GT-54115, New York, NY.

[48] P. Chiesa, S. Consonni, T.G. Kreutz, R.H. Williams, Co-production of hydrogen, electricity and CO_2 from coal using commercially-ready technology, in: Proceedings of the Second Annual Conference on Carbon Sequestration, Washington, May 5–8, 2003.
[49] http://www.matche.com.
[50] R.F. Bohem, Design Analysis of Thermal Systems, John Wiley and Sons, 1987.
[51] T.P. Chen, J.D. Wright, K. Krist, SOFC system analysis, GRI study.